Holistic Adaptive Multi-Model Predictive Control for the Path Following of 4WID Autonomous Vehicles

Yixiao Liang, Yinong Li, Amir Khajepour, and Ling Zheng

***Abstract*—This paper presents a novel adaptive multiple-model predictive control (MPC) scheme for Four-Wheel Independent Drive (4WID) autonomous vehicles with a holistic structure. Firstly, the combined vehicle-path model is established. To ensure the real-time performance of MPC, the coupling relationships in the control output and the longitudinal/lateral motions are well decoupled, in this way a linear integrated model is utilized as the internal model of the controller. Then, the holistic MPC is proposed to acquire the steering angle and the force on each corner. Based on the advantages of the proposed structure, a weight adaptive mechanism is introduced to improve the handling ability of the controller to various driving conditions, especially some extreme conditions. For the uncertainties in tire cornering stiffness, a multiple-model adaptive law is designed with its convergence proved by Lyapunov theory. Numerical results based on Carsim-Simulink co-simulation platform demonstrate the effectiveness and superiority of the proposed control method in both normal and extreme driving conditions.**

***Index Terms*—Autonomous vehicles, path following control, holistic control structure, model predictive control, adaptive control, multiple-model theory.**

I. Introduction

AUTONOMOUS vehicles have shown great potential in improving driving safety and traffic throughput [1]–[2]. Recent years, worldwide attentions from academia, industry, and governments are attracted to this area [3]. The development of autonomous driving requires technologies involving multiple disciplines including engineering, computer science and mathematics [4]. Path following control, referring to enable the autonomous vehicle to track the reference path, is one of the basic and key technologies for autonomous driving. Considerable methods have been proposed for this issue, such as Proportion Integral Derivative (PID) control [5], pure-pursuit control [6], sliding mode control (SMC) [7], fuzzy control [8], optimal control [9]–[10] and model predictive control (MPC) [11]–[12]. Among these methods, MPC is supposed to be the most promising method owing to its ability to systematically deal with multiple constraints, and the problem on real-time performance has been alleviated a lot thanks to the development in optimization algorithms and higher performance Central Processing Unit (CPU) [13]. Except for path following control, MPC is also extensively applied in many areas of vehicle control, including suspension control [14]–[15] and dynamics stability control [16].

The above researches consider the path following of autonomous vehicles with traditional powertrain, and the only lateral control output is the steering angle. Recent years, with the development of electric drive technology [17], four-wheel independently driving (4WID) vehicles have earned considerable attention. The redundant control output, generated by the torque differences between left and right in-wheel motors, also known as active yaw moment, can strongly improve vehicle cornering performance, which has been widely studied and evaluated in previous researches on vehicle stability control [18]–[20]. Many advanced control methods including LPV/gain scheduled/H∞ [21]–[24], μ synthesis [25], SMC [26] and MPC [27]–[28] have been introduced to coordinate the steering and driving/braking of 4WID vehicles, which further improve the control performance. These benefits have inspired researches on the path following control of 4WID autonomous vehicles. Chatzikomis *et al.* [29] analyze multiple sets of configuration on autonomous vehicles, the results confirm that the involvements of the active yaw moment do improve the path following performance. Ren *et al.* [30] present an integrated control scheme for the 4WID autonomous vehicle, the steering angle is calculated by an MPC controller while a sliding mode controller is presented to obtain the active yaw moment. In [31], an optimal control law is presented to generate the front steering angle and the external yaw-moment by feeding back the vehicle dynamics and road-related parameters. To prevent the vehicle from transgressing the safety bound in path following, a hyperbolic projection method is proposed by Hu *et al.* [32], and the control outputs for actuators are obtained by an adaptive linear quadratic regulator (LQR) controller. Wang *et al.* [33] propose a modified composite nonlinear feedback strategy for 4WID autonomous vehicle to improve the

Manuscript received July 1, 2020; revised November 1, 2020 and December 14, 2020; accepted December 16, 2020. Date of publication December 21, 2020; date of current version February 12, 2021. This work was supported in part by the Key Research Program of the Ministry of Science and Technology under Grant 2017YFB0102603-3, in part by the National Nature Science foundation of China under Grant 51875061, in part by the Chongqing Science and Technology Program Project Basic Science and Frontier Technology (cstc2018jcyjAX0630), China Scholarship Council (201906050066), and in part by the Graduate Scientific Research and Innovation Foundation of Chongqing (CYB19063). The review of this article was coordinated by Prof. N. Kato. *(Corresponding author: Yinong Li.)*

Yixiao Liang is with the State Key Laboratory of Mechanical Transmissions and the School of Automotive Engineering, Chongqing University, Chongqing 400044, China, and also with the Department of Mechanical and Mechatronics Engineering, University of Waterloo, ON N2L3G1, Canada (e-mail: liangyixiao1119@foxmail.com).

Yinong Li and Ling Zheng are with the State Key Laboratory of Mechanical Transmissions and the School of Automotive Engineering, Chongqing University, Chongqing 400044, China (e-mail: ynli@cqu.edu.cn; zling@cqu.edu.cn).

Amir Khajepour is with the Department of Mechanical and Mechatronics Engineering, University of Waterloo, ON N2L3G1, Canada (e-mail: a.khajepour@uwaterloo.ca).

Digital Object Identifier 10.1109/TVT.2020.3046052

0018-9545 © 2020 IEEE. Personal use is permitted, but republication/redistribution requires IEEE permission.
See https://www.ieee.org/publications/rights/index.html for more information.

Authorized licensed use limited to: University of Maryland College Park. Downloaded on October 10,2021 at 16:55:00 UTC from IEEE Xplore. Restrictions apply.

transient performance and eliminate the steady-state errors in path-following control. In [34], a linear time varying (LTV)-based model predictive controller (MPC) with a fuzzy factor is proposed to acquire the wheel steering angle and active yaw moment, then a pseudo inverse (PI) low-level control allocation law is designed to realize the tracking of active yaw moment and the management of the redundant tire actuators.

In general, existing researches on the path following control of 4WID are based on a classical hierarchical structure, usually an upper level controller is designed to obtain the steering angle and the generalized forces, while a lower level controller is presented to allocate the generalized forces to four wheels. This structure performs well in most driving conditions. However, the researches on vehicle dynamics control have shown that in some extreme conditions, inevitable conflicts will appear between the upper level controller and the lower level allocator, since the actuators encounter difficulties to fulfill the generalized forces calculated by the upper level controller [35]. For this problem, some researches propose a holistic structure [36]–[37]. In this structure, the control commands on each corner are calculated directly without the generalized forces acting as intermediate variables. Therefore, the vehicle can achieve better performance in these extreme conditions. However, compared with the hierarchical structure, the holistic structure requires more complicated dynamics models, including nonlinear model [38]–[39] or linear model with complex mathematical relationships [40]. The complexity in internal models may highly increase the computation burden of the controllers. Moreover, some new problems need to be solved when transplanting the holistic structure to the path following control of 4WID autonomous vehicles, such as the coupling between longitudinal and lateral motions, as well as the coupling between steering angle and the torque commands on the steering wheels.

It is worth mentioning that even under well-designed decision and path planning strategies, some extreme driving conditions cannot be entirely avoided by autonomous vehicle, e.g., to avoid a suddenly appeared obstacle while driving on high speed. Some researches [41]–[43] set "envelopes" to describe the road safety constraints as well as the dynamics stability constraints, then utilize MPC to deal with this multiple-constraints problem. When the two objectives conflict with each other, the path following objective is prioritized by setting a very large weight on its slacking variable. Nevertheless, it is known that the road safety constraints may violently conflict with the dynamics stability in some emergency situations [44], which may cause the optimization infeasible. The vehicle may lose dynamics stability or controllability if they are forced to follow the reference path. When this happens, the cooperation of the longitudinal motion is necessary. But the cooperation mechanism needs to be designed very carefully because in these situations the vehicles are very close to their adhesive limits.

Additionally, the vehicle dynamics model is a complex system with nonlinearity and uncertainties owing to the complex characteristics of tire [45]. For the lateral dynamics control, the main uncertainties come from the variation of tire cornering stiffness, which is influenced by many factors such as road adhesion, normal load and tire slip angle [46]. The mainstream solutions for this problem are robust control methods [47]–[48], which have been proved to be very effective when the actual values deviate a lot from the calibration values defined in controllers. However, these methods may be too conservative because of worst-case consideration [49].

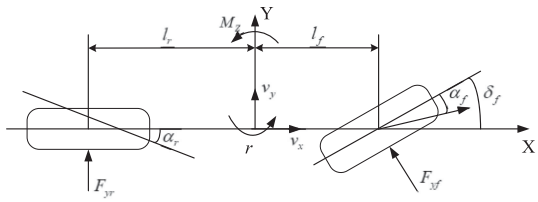

Fig. 1. Simplified single track vehicle model.

To this end, this paper proposes a novel holistic multiple-model predictive controller for the path following of 4WID autonomous vehicles. The main contribution of this paper lies on the following aspects: (1). The coupling terms mentioned above are well decoupled in the system modeling, so the proposed holistic controller owes a linear form without complex mathematical relationships, which is beneficial to release the computation burden of MPC. (2). A weight adaptive mechanism is designed in the holistic MPC to coordinate the longitudinal motions and regulate the slip ratio of each wheel, in this way the performance of autonomous vehicles in extreme conditions can be ensured. (3). For the uncertainties in tire cornering stiffness, an adaptive law based on multiple model theory is designed to increase the accuracy of the internal dynamics model without introducing conservativeness. Comprehensive case studies based on the co-simulation platform of MATLAB/Simulink and Carsim show the effectiveness and unique superiority of the proposed method.

The rest of this paper is organized as follows: The modeling of the system is presented in Section II. In Section III, the holistic MPC with adaptive mechanisms is proposed, followed by the multiple-model adaptive method for model uncertainties. Simulation results are illustrated in Section IV. Section V is the conclusion.

II. System Modeling

For the controller design, as shown in Fig. 1, a simplified single track vehicle model is introduced based on the following assumptions: (1) The steering angle of front wheels is small; (2) The difference of steering angle between left and right wheels caused by Ackermann steering geometry is neglected [39]. The state-space form of the simplified single-track model is obtained as follows:

$$\begin{bmatrix} \dot{v}_y \\ \dot{r} \end{bmatrix} = \begin{bmatrix} -\frac{(c_f+c_r)}{mv_x} & -v_x - \frac{(l_f c_f - l_r c_r)}{mv_x} \\ -\frac{c_f l_f - c_r l_r}{I_z v_x} & -\frac{c_f {l_f}^2 + c_r {l_r}^2}{I_z v_x} \end{bmatrix} \begin{bmatrix} v_y \\ r \end{bmatrix} + \begin{bmatrix} \frac{c_f}{m} & 0 \\ \frac{l_f c_f}{I_z} & \frac{1}{I_z} \end{bmatrix} \begin{bmatrix} \delta_f \\ M_z \end{bmatrix} \quad (1)$$

where m is the mass of vehicle and I_z is the moment of inertia about vertical access; v_x, v_y and r are the longitudinal velocity, lateral velocity and yaw rate of the vehicle, respectively; c_f and

Authorized licensed use limited to: University of Maryland College Park. Downloaded on October 10,2021 at 16:55:00 UTC from IEEE Xplore. Restrictions apply.

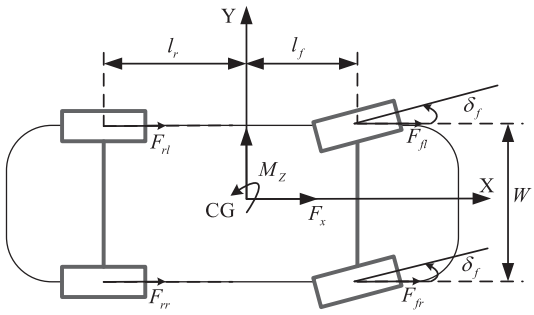

Fig. 2. Extended vehicle single track model.

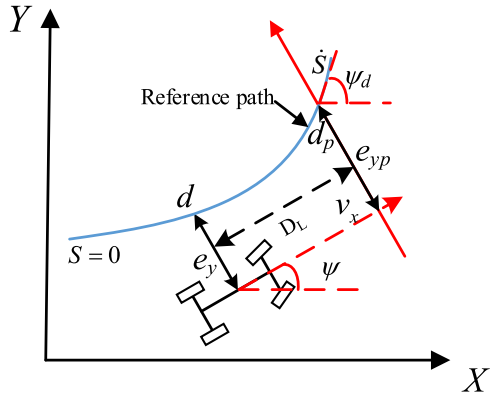

Fig. 3. Path following model.

c_r are the cornering stiffness of front and rear tires, respectively; δ_f is the front wheel steering angle, and M_z is the active yaw moment, as shown in the extended vehicle single track model in Figure. 2, it is generated by the torque difference between left and right wheels:

$$\begin{aligned} M_z = & -F_{xlf}\frac{W}{2} + F_{xrf}\frac{W}{2} - F_{xlr}\frac{W}{2} + F_{xrr}\frac{W}{2} \\ \approx & -\frac{T_{xlf}\cos\delta_f}{r_w}\frac{W}{2} + \frac{T_{xlf}\cos\delta_f}{r_w}\frac{W}{2} - \frac{T_{xlr}}{r_w}\frac{W}{2} \\ & + \frac{T_{xrr}}{r_w}\frac{W}{2} \end{aligned} \tag{2}$$

where W is the track width of vehicle, r_w is the wheel radius; T_{xlf}, T_{xrf}, T_{xlr}, T_{xrr} are the torques on the front-left, front-right, rear-left, rear-right wheel, respectively; F_{xlf}, F_{xrf}, F_{xlr}, F_{xrr} are the forces on the center of each wheel, respectively. It is worth mentioning that F_{xlf}, F_{xrf}, F_{xlr}, F_{xrr} are the decomposed component of tire force on the longitudinal direction of vehicle body. Here, since the term $\sin\delta_f$ is small in most driving conditions, the decomposed component of tire lateral forces on the longitudinal direction of vehicle body is ignored.

To reflect the relationships between the vehicle and reference path, an error-based path following model is introduced as shown in Fig. 3, where e_y is the lateral error from vehicle center of gravity (CG) to the closest point d on the desired path. For the controller design, a preview mechanism is introduced, and D_L is the preview distance. e_{yp} is the lateral error from vehicle center of gravity (CG) to the preview point d_p on the desired path, ψ_d is the desired heading angle while ψ is the actual heading angle of vehicle. The heading error can be defined as $\Delta\psi = \psi - \psi_d$. The relationship between path and vehicle based on Serret-Frenet equation and in-road assumption can be modeled as follows [23]:

$$\begin{cases} \dot{e}_{yp} = v_x\Delta\psi + v_y + rD_L \\ \Delta\dot{\psi} = \dot{\psi} - \dot{\psi}_d = r - \rho(d)v_x \end{cases} \tag{3}$$

Moreover, the preview distance D_L has the following relationship with the velocity of vehicle:

$$D_L = \begin{cases} D_{\text{low}} & v_x \le v_{xthel} \\ v_x\Delta t & v_{xthel} < v_x < v_{xtheh} \\ D_{high} & v_x \ge v_{xtheh} \end{cases} \tag{4}$$

where Δt is the preview time, D_{low} and D_{high} are the lower and upper thresholds of D_L, respectively, v_{thel} is the lower limit of longitudinal velocity in generating the preview distance while v_{theh} is the upper limit of longitudinal velocity. Here, Δt is set as 0.4 s, D_{low} and D_{high} are set as 2 m and 12 m, respectively, v_{thel} *and* v_{theh} are set as 5 m/s and 30 m/s, respectively.

Combine Eq. (1) and Eq. (3), a combined model of path following and vehicle dynamics can be derived as follows:

$$\begin{cases} \dot{e}_{yp} = v_x\Delta\psi + v_y + D_L r \\ \Delta\dot{\psi} = r - \rho(d)v_x \\ \dot{v}_y = -\frac{c_f+c_r}{mv_x}v_y + \left(-v_x - \frac{l_f c_f - l_r c_r}{mv_x}\right)r + \frac{c_f}{m}\delta_f \\ \dot{r} = \frac{l_r c_r - l_f c_f}{I_z v_x}v_y - \frac{c_f {l_f}^2 + c_r {l_r}^2}{I_z v_x}r + \frac{l_f c_f}{I_z}\delta_f + \frac{1}{I_z}M_z \end{cases} \tag{5}$$

To avoid complex coupling relationships that will lead to nonlinearity and tremendously increase the computation burden of controller, for the longitudinal velocity tracking problem, a simplified model is given as follows:

$$\begin{cases} \dot{e}_x = \frac{F_{xt}}{m} - a_{xd} \\ e_x = v_x - v_{xd} \end{cases} \tag{6}$$

where v_{xd} is the reference velocity, a_{xd} is the reference acceleration which can be acquired by differentiating v_{xd}, F_{xt} is the total longitudinal forces that can be expressed as follows:

$$\begin{aligned} F_{xt} &= F_{xlf} + F_{xrf} + F_{xlr} + F_{xrr} \\ &\approx \frac{T_{xlf}\cos\delta_f}{r_w} + \frac{T_{xrf}\cos\delta_f}{r_w} + \frac{T_{xlr}}{r_w} + \frac{T_{xrr}}{r_w} \end{aligned} \tag{7}$$

where r_w is the radius of each wheel.

Moreover, for a holistic structure, the generalized forces such as F_{xt} and M_z should be replaced by the control inputs on each wheel. It should be noted that the torques of the steering wheel are coupled with the steering angle. For the front wheels, their longitudinal direction is not the same as the longitudinal direction of vehicle body when the vehicle is steering. If the forces proposed by the driven torques are directly integrated in the predictive model, they have to be decomposed into the longitudinal/lateral directions of vehicle body by multiplying $\sin\delta_f$/$\cos\delta_f$. For a holistic control structure, this coupling will immensely increase the complexity of the system and make the model nonlinear. To ensure a linear structure for controller design, the longitudinal forces at each wheel center are utilized instead of the torques on each wheel, in this way the decoupling between the steering angle and the control command of motors is achieved.

Authorized licensed use limited to: University of Maryland College Park. Downloaded on October 10,2021 at 16:55:00 UTC from IEEE Xplore. Restrictions apply.

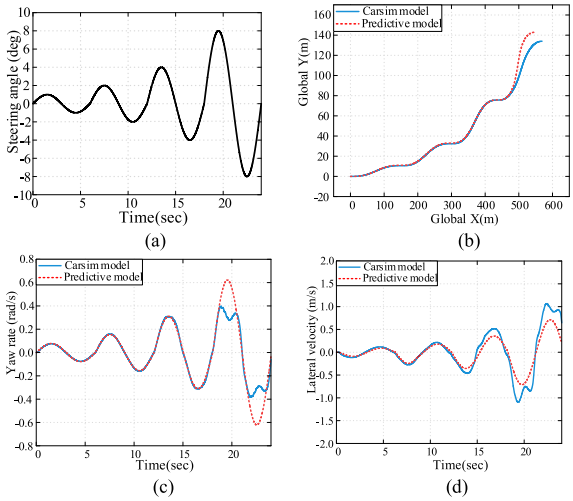

Fig. 4. Comparison between predictive model and Carsim model: (a) steering angle, (b) global trajectory, (c) yaw rate, (d) lateral velocity.

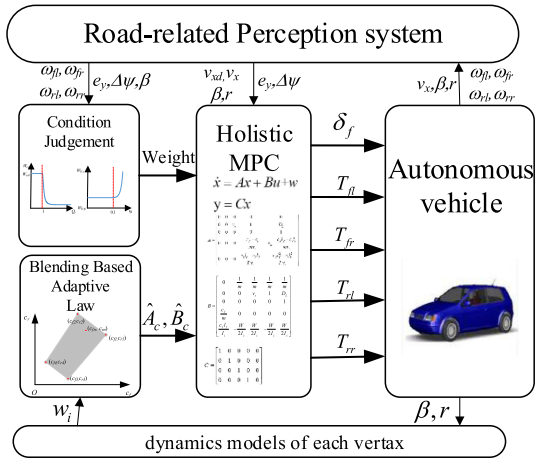

Fig. 5 Overall structure of the Multiple-model holistic adaptive predictive control.

Combine Eq. (2) with Eq. (5)∼Eq. (7), and manipulate the combined model into state-space form, The state vector is defined as $x = [\, e_x \; e_{yp} \; \Delta\psi \; v_y r]^T$, the control input is $u = [\delta_f \; F_{xlf} \; F_{xrf} \; F_{xlr} \; F_{xrr}]$, the disturbance is defined as $w = [-a_{xd} \; v_x\rho \; 0 \; 0 \; 0]^{\mathrm{T}}$, and the output of the system is defined as $\mathrm{y} = [\, e_x \; e_{yp} \; \Delta\psi \; v_y]^{\,T}$. The state-space form of the combined system can be expressed as follows:

$$\begin{aligned} \dot{x} &= Ax + Bu + w \\ \mathrm{y} &= Cx \end{aligned} \tag{8}$$

where

$$A = \begin{bmatrix} 0 & 0 & 0 & 0 & 0 \\ 0 & 0 & v_x & 1 & D_L \\ 0 & 0 & 0 & 0 & 1 \\ 0 & 0 & 0 & -\frac{c_f + c_r}{m v_x} & -v_x - \frac{c_f l_f - c_r l_r}{m v_x} \\ 0 & 0 & 0 & \frac{c_r l_r - c_f l_f}{I_z v_x} & -\frac{c_f l_f^2 + c_r l_r^2}{I_z v_x} \end{bmatrix},$$

$$B = \begin{bmatrix} 0 & \frac{1}{m} & \frac{1}{m} & \frac{1}{m} & \frac{1}{m} \\ 0 & 0 & v_x & 1 & D_L \\ 0 & 0 & 0 & 0 & 1 \\ \frac{c_f}{m} & 0 & 0 & 0 & 0 \\ \frac{c_f l_f}{I_z} & -\frac{W}{2I_z} & \frac{W}{2I_z} & -\frac{W}{2I_z} & \frac{W}{2I_z} \end{bmatrix},$$

$$C = \begin{bmatrix} 1 & 0 & 0 & 0 & 0 \\ 0 & 1 & 0 & 0 & 0 \\ 0 & 0 & 1 & 0 & 0 \\ 0 & 0 & 0 & 1 & 0 \end{bmatrix}.$$

It is worth mentioning that by choosing e_x as the state of the system, the longitudinal and lateral motions can be decoupled, which is very beneficial to release the computation burden of MPC.

To evaluate the accuracy of the predictive model, a comparison is conducted between the established model and Carsim model, as shown in Fig. 4. The velocity is set as 90 km/h and the road adhesive parameter is 0.8. A slalom steering maneuver with periodically increasing magnitude is given in Fig. 4(a). By this steering input, the characteristics under slight, large and fierce steering maneuvers can be intuitively observed. The global trajectory, yaw rate and lateral velocity are shown in Fig. 4(b), (c) and (d), respectively. One can see that during the first three periods, the responses of the predictive model can match well with the Carsim model. Although during the third period, a difference appears in the lateral velocity response, it is within acceptable range. This can persuasively verify the accuracy of the predictive model. However, during the fourth period with fierce steering, it is shown that the difference between predictive model and Carsim model becomes obvious. This is because of the fact that in the intensive maneuver, the tire can no longer stay in its linear region, so the difference between real tire cornering stiffness and the nominal value defined in the predictive model becomes very large. The significant model error will affect the feasibility of MPC. This will be considered in the controller design.

III. Controller Design

The overall structure of the controller based on holistic MPC is shown in Fig. 5. To deal with some extreme situations, a condition judgement module is introduced with the ability to adjust the weight parameters according to driving conditions. Moreover, a blending based adaptive law is proposed based on the multi-model adaptive theory for the model uncertainties. At each sampling instant, the supporting modules including the weight adaptive mechanism and the blending adaptive law update the adaptive weight and the identified system matrixes. In this way, the holistic controller can be adaptive to various driving conditions and model uncertainties.

A. Holistic Model Predictive Path Following Controller Design

For the design of MPC, a discrete model is required. Thus, the continuous model in Eq. (8) is discretized as follows:

$$\begin{aligned} x(k+1) &= A_d x(k) + B_d u(k) + \Delta T w(k) \\ \mathrm{y} &= C_d x \end{aligned} \tag{9}$$

Authorized licensed use limited to: University of Maryland College Park. Downloaded on October 10,2021 at 16:55:00 UTC from IEEE Xplore. Restrictions apply.

where A_d, B_d, C_d are the discrete state equations that can be simplified as:

$$A_d = I + A \times \Delta T,\ B_d = B \times \Delta T,\ C_d = C \tag{10}$$

where ΔT is the time step of the MPC controller, here ΔT is set as 0.01s.

The states in the prediction horizon can be iterated as follows:

$$\begin{aligned} x(k+2) &= A_d x(k+1) + B_d u(k+1) + \Delta T w(k+1) \\ &= A_d^2 x(k) + A_d B_d u(k) + A_d \Delta T w(k) \\ &\quad + B_d u(k+1) + \Delta T w(k+1) \\ &\vdots \\ x(k+N_c) &= A_d^{N_c} x(k) + A_d^{N_c-1} B_d u(k) + A_d^{N_c-1} \Delta T w(k) \cdots \\ &\quad + B_d u(k+N_c-1) + \Delta T w(k+N_p) \\ &\vdots \\ x(k+N_p) &= A_d^{N_p} X(k) + A_d^{N_p-1} B_d u(k) + A_d^{N_p-1} \Delta T w(k) \\ &\quad + \cdots + A_d^{N_p-N_c} B_d u(k+N_c-1) \\ &\quad + A_d^{N_p-N_c} \Delta T w(k+N_c-1) + \cdots \Delta T w(k+N_c-1) \end{aligned} \tag{11}$$

where N_p is the step of the prediction horizon, N_c is the step of the control horizon. Here, Zero-Order-Hold (ZOH) is utilized for two consecutive instants.

The output of the state space model in the predictive horizon can be calculated as:

$$Y(k) = C_p x(k) + D_p U(k) + E_p W(k) \tag{12}$$

where $Y(k) = [y(k), y(k+1) \ldots, y(k+N_p)]^T$, unnumbered equation, shown at the bottom of this page,

The optimization function of the MPC can be defined as follows:

$$\min J = (Y - Y_{des})^T Q (Y - Y_{des}) + U^T R U \tag{13}$$

where Q is the weight matrix of system output, R is the weight matrix of control input, Y_{des} is the desired system output, these matrixes have the following definition:

$$Q = \begin{bmatrix} Q_1 & & & \\ & Q_2 & & \\ & & \cdots & \\ & & & Q_{N_p} \end{bmatrix}_{N_p \times N_p} \quad R = \begin{bmatrix} R_1 & & & \\ & R_2 & & \\ & & \cdots & \\ & & & R_{N_c} \end{bmatrix}_{N_c \times N_c}$$

$$Q_i = \begin{bmatrix} W_{ex} & & & \\ & W_{ey} & & \\ & & W_{\Delta\psi} & \\ & & & W_{vy} \end{bmatrix}$$

$$R_i = \begin{bmatrix} W_{\delta} & & & & \\ & W_{Ffl} & & & \\ & & W_{Ffr} & & \\ & & & W_{Frl} & \\ & & & & W_{Frr} \end{bmatrix}$$

$$Y_{des} = \begin{bmatrix} Y_{des1} \\ Y_{des2} \\ \cdots \\ Y_{desN_p} \end{bmatrix}_{N_p \times 1} \quad Y_{desi} = \begin{bmatrix} v_{xd} \\ 0 \\ 0 \\ 0 \end{bmatrix} \tag{14}$$

In the weighing matrix of system output, W_{ex} is the weight of velocity tracking, W_{ey} is the weight of lateral error, $W\Delta_{\psi}$ is the weight of heading error, W_{vy} is the weight of lateral velocity; while in the weighing matrix of control output, W_{δ} is the weight of steering angle, W_{Fij} is the weight of the longitudinal forces at the center of each wheel.

An adaptive mechanism for the weighting system is proposed to improve the performance of vehicle under varies driving conditions, especially some extreme situations. For the weighting

---

$$\begin{aligned} X(k) &= [x(k), x(k+1) \ldots, x(k+N_p)]^T \\ U(k) &= [u(k), u(k+1) \ldots, u(k+N_c)]^T \\ W(k) &= [\Delta T w(k), \Delta T w(k+1) \ldots, \Delta T w(k+N_p)]^T \\ C_p &= \left[C_d A_d; C_d A_d^2; \ldots C_d A_d^{N_p-1} \right]^T \\ D_p &= \begin{bmatrix} C_d B_d & 0 & \cdots & 0 & 0 \\ & & \vdots & & \\ C_d A_d^{N_c} B_d & C_d A_d^{N_c-1} B_d & \cdots & C_d A_d B_d & C_d B_d \\ & & \vdots & & \\ C_d A_d^{N_p-1} B_d & C_d A_d^{N_p-2} B_d & \cdots & C_d A_d^{N_p-N_c+1} B_d & C_d A_d^{N_p-N_c} B_d \end{bmatrix} \\ E_p &= \begin{bmatrix} C_d & 0 & \cdots & 0 & 0 \\ & & \vdots & & \\ C_d A_d^{N_p-1} & C_d A_d^{N_p-2} & \cdots & C_d A_d & C_d \end{bmatrix} \end{aligned}$$

Authorized licensed use limited to: University of Maryland College Park. Downloaded on October 10,2021 at 16:55:00 UTC from IEEE Xplore. Restrictions apply.

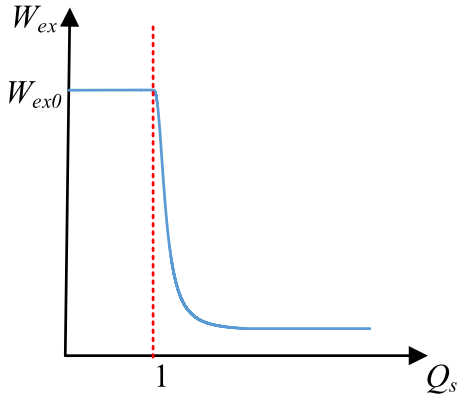

Fig. 6. The relationships between Q_s and W_{ex}.

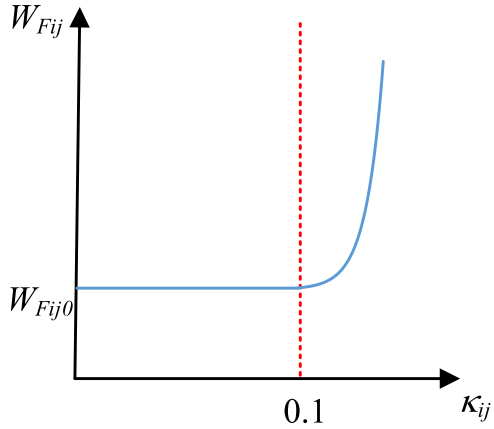

Fig. 7. The relationships between κ_{ij} and W_{Fij}.

matrix on system output, an adaptive mechanism on the weight of velocity tracking is designed as follows according to the hyperbolic tangent function:

$$\begin{aligned} Q_s &= \max\left(\frac{|e_y|}{e_{ythe}}, \frac{|\Delta\psi|}{\Delta\psi_{the}}, \frac{|\beta|}{\beta_{the}}\right) \\ &\text{If } Q_s \le 1 : W_{ex} = W_{ex0} \\ &\text{else}: \quad W_{ex} = a_s + b_s \tanh\left(\frac{k_s}{Q_s}\right)^{c_s} \end{aligned} \tag{15}$$

where e_{ythe}, $\Delta\psi_{the}$, β_{the} is the defined thresholds for lateral error, heading error and side slip angle, respectively; W_{ex0} is the origin weight of velocity tracking, a_s, b_s, c_s and k_s are the parameters of the weight adaptive mechanism, tanh() is hyperbolic tangent function with the following definition:

$$\tanh(s) = \frac{e^s - e^{-s}}{e^s + e^{-s}} \tag{16}$$

By tuning parameters a_s, b_s, c_s and k_s through trial and error process, the relationships between Q_s and W_{ex} are shown in Fig. 6. When Q_s becomes larger than 1, which means the controller has difficulties in maintaining the path tracking performance or dynamics stability, the weight W_{ex} will decrease dramatically from its origin value W_{ex0}. By choosing a small W_{ex}, the velocity tracking is set in a low priority. This can help ensure the controllability of lateral controller and maintain the dynamics stability of the vehicle. Moreover, to further ensure the lateral safety, a time lag τ is introduced when the W_{ex} is going to restore to its nominal value W_{ex0} after an extreme maneuver has just been finished.

A weight adaptive mechanism is also proposed for the control output to prevent oversized slip ratio on each wheel. The mechanism is designed as follows:

$$\begin{aligned} &\kappa r_{ij} = |\kappa_{ij}| \\ &\text{if } \kappa r_{ij} <= 0.1 : \quad W_{Fij} = W_{Fij0} \\ &\text{else}: \; W_{Fij} = W_{Fij0} * e^{k_w(\kappa r_{ij} - 0.1)} \end{aligned} \tag{17}$$

where W_{Fij0} is the origin weight on the longitudinal force of each wheel, k_w is parameter of the weight adaptive mechanism, κ_{ij} is the slip ratio of each wheel which can be calculated as follows:

$$\kappa_{ij} = \begin{cases} 1 - \frac{v_x}{r_w\omega_{ij}}, & v_x < r_w\omega_{ij} \\ \frac{r_w\omega_{ij}}{v_x} - 1, & v_x > r_w\omega_{ij} \end{cases} \tag{18}$$

where ω_{ij} is the wheel speed.

The relationship between κ_{ij} and W_{Fij} is tuned to meet the control requirements, as shown in Fig. 7. When the absolute value of slip ratio is larger than 0.1, W_{Fij} will grow sharply from its origin value W_{Fij0}, which means the forces on the corresponding wheel will be released rapidly. In this way the oversized slip ratio can be well prevented, which is very beneficial to the controllability of the autonomous vehicle.

The constraints on control output are defined as follows:

$$U_{\min} \le U \le U_{\max} \tag{19}$$

where $U_{\min}$ and $U_{\max}$ are the lower and upper bound of the control output, respectively, with the following definition:

$$\begin{aligned} U_{\min} &= \begin{bmatrix} U_{\min 1} \\ U_{\min 2} \\ \cdots \\ U_{\min Nc} \end{bmatrix}_{N_c \times 1} \qquad U_{\max} = \begin{bmatrix} U_{\max 1} \\ U_{\max 2} \\ \cdots \\ U_{\max Nc} \end{bmatrix}_{N_c \times 1} \\ U_{\min 1} &= \max(u_{\min}, u_p - \Delta u_{\max}) \\ U_{\max 1} &= \min(u_{\max}, u_p + \Delta u_{\max}) \\ U_{\min 2\cdots N_c} &= u_{\min} \quad U_{\max 2\cdots N_c} = u_{\max} \end{aligned} \tag{20}$$

where u_p is the control output at last calculation interval, $\Delta u_{\max}$ is the maximum allowable variation of control output during each sampling time. Compared with other control outputs in the prediction horizon, the first control output is constrained not only by the minimum and maximum control output but also by the allowable variation from the last control output in order to constrain the rate of change.

Moreover, to ensure the driving safety, the constraints on system output is also proposed as follows, with a slack variable ε introduced to prevent unsolvable problem:

$$Y_{\min} - \varepsilon I_{Np*1} \le Y \le Y_{\max} + \varepsilon I_{Np*1} \tag{21}$$

Authorized licensed use limited to: University of Maryland College Park. Downloaded on October 10,2021 at 16:55:00 UTC from IEEE Xplore. Restrictions apply.

Thus, the cost function in Eq. (21) can be rewritten as follows:

$$\begin{aligned} &\min J = (Y - Y_{des})^T Q (Y - Y_{des}) + U^T R U + \rho\varepsilon^2 \\ &\text{s.t. } U_{\min} \le U \le U_{\max} \\ &Y_{\min} - \varepsilon I_{Np*1} \le Y \le Y_{\max} + \varepsilon I_{Np*1} \end{aligned} \tag{22}$$

where ρ is the weighting matrix to penalize the slacking variable.

The optimization problem in Eq. (22) can be transformed into quadratic programming (QP) form as:

$$\begin{aligned} &\min J = \frac{1}{2}\hat{U}^T G_k \hat{U} + H_k \hat{U} \\ &\text{s.t. } \hat{U}_{\min} \le \hat{U} \le \hat{U}_{\max} \\ &A_{\text{cons}}\hat{U} \le B_{\text{cons}} \end{aligned} \tag{23}$$

where

$$G_k = 2\begin{bmatrix} D_p^T Q D_p + R & 0 \\ 0 & \rho \end{bmatrix}$$

$$H_k = 2\begin{bmatrix} (C_p X(k) - Y_{\text{des}})^T Q D_p \\ 0 \end{bmatrix}$$

$$\hat{U} = \begin{bmatrix} U \\ \varepsilon \end{bmatrix}, \hat{U}_{\max} = \begin{bmatrix} U_{\max} \\ \varepsilon_{\max} \end{bmatrix}, \hat{U}_{\min} = \begin{bmatrix} U_{\min} \\ 0 \end{bmatrix},$$

$$A_{cons} = \begin{bmatrix} D_p & -1_{N_p\times 1} \\ -D_p & -1_{N_p\times 1} \end{bmatrix}, B_{cons} = \begin{bmatrix} Y_{\max} - C_p x(k) \\ Y_{\min} + C_p x(k) \end{bmatrix}.$$

It should be noted that the controller utilizes the longitudinal force on each wheel as the control output for each motor, which is an indirect command. So a simple transition should be appended before the command reaches actuators:

$$\begin{aligned} T_{xlf} = \frac{F_{xlf} r_w}{\cos\delta_f},\ T_{xrf} = \frac{F_{xrf} r_w}{\cos\delta_f}, T_{xlr} \\ = F_{xlr} r_w, T_{xrr} = F_{xrr} r_w \end{aligned} \tag{24}$$

Remark 1: Due to the longitudinal-slip characteristics of tires [50], it is known that the relationships between the force and the torque in Eq. (24) is not accurate, especially when the slip ratio is high. However, excessive slip ratio can be avoided because of the weight adaptive mechanism proposed in Eq. (18). Thus, it is persuasive that the accuracy of the relationships in Eq. (24) is acceptable in this research.

Remark 2: For the proposed method, although some weight parameters are adaptive, their value still remain unchanged during the iteration process of MPC. Specifically, after the values are decided by the condition judgement module, they will remain unchanged during different instants of one iteration, which is the same as normal MPC. And to ensure the stability of the controller, the maximum/minimum value of the adaptive weight parameters should be decided carefully.

B. Multiple Model Adaptive Predictive Controller

It is known that the vehicle is a complex system with multiple uncertainties. For the path following control, the most significant uncertainties come from the cornering stiffness, which varies according to many factors such as road adhesive condition, vertical load and so on. To deal with this problem, a polytope

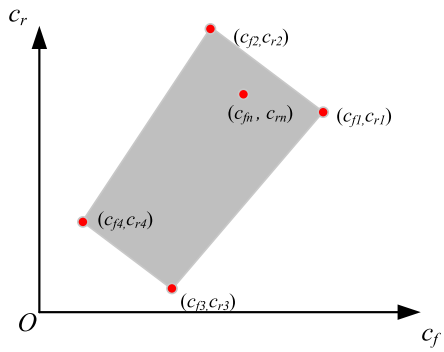

Fig. 8. Convex polytope of tire cornering stiffness.

with four vertexes named (c_{f1}, c_{r1}), (c_{f2}, c_{r2}), (c_{f3}, c_{r3}), (c_{f4}, c_{r4}) is formed to cover all the possible perturbations of cornering stiffness, while (c_{fn}, c_{rn}) is the calibration cornering stiffness, as shown in Fig. 8.

Based on the multiple-model theory [51], any uncertainties of cornering stiffness within the shadow area in Fig. 6 can be linearly expressed by the four vertexes, as follows:

$$A_p(\lambda)x_p(t) + B_p(\lambda)u(t) = \sum_{i=1}^{4} w_i(t)\left[A_i x_p(t) + B_i u(t)\right] \tag{25}$$

where λ is the parameter to denote the uncertainty parameters in the model, A_p and B_p denote the system matrix in Eq. (1), $w_i(t)$ is the weight of the corresponding model at time instant t that satisfies the following condition:

$$\sum_{i=1}^{4} w_i(t) = 1,\ w_i(t) \ge 0 \tag{26}$$

According to Eq. (25), it is clear that the estimation of the unknown weights w_i can be equivalent to the identification of the unknown matrices $A_p(\lambda)$ and $B_p(\lambda)$. For the online identification problem, the classic form of the dynamics model can be expressed in the form of the linear parametric model, as follows [52]:

$$\begin{aligned} z(t) &= \Theta_p(\lambda)\Phi(t) \\ \Theta_p(\lambda) &= [A_p(\lambda)\quad B_p(\lambda)] \\ \Phi = \frac{1}{s+\gamma}\begin{bmatrix} x_p \\ u \end{bmatrix}, z &= \frac{s}{s+\gamma}x_p, \quad \gamma > 0 \end{aligned} \tag{27}$$

where s denotes the differentiation operator and γ is a constant design parameter. The system is transformed from state-space form to the linear parametric form since the latter is suitable for applying gradient descent based method. Similarly, the fixed model of each vertex can be parameterized as:

$$\begin{aligned} z_i(t) &= \Theta_i\Phi(t) \\ \Theta_i &= [A_i\quad B_i]\, i = 1, \cdots, N \end{aligned} \tag{28}$$

where $z_i = \frac{s}{s+\lambda}x_i$. Then, the estimation errors of the vertex-model are defined as:

$$\varepsilon_i(t) = z(t) - \Theta_i\Phi(t), \quad i = 1, \cdots, N \tag{29}$$

Authorized licensed use limited to: University of Maryland College Park. Downloaded on October 10,2021 at 16:55:00 UTC from IEEE Xplore. Restrictions apply.

Based on Eq. (25) and Eq. (26), the following relationships can be derived:

$$\Theta_p(t) = \sum_{i=1}^{4} w_i(t)\Theta_i$$

$$\sum_{i=1}^{4} w_i(t)\varepsilon_i(t) = 0 \tag{30}$$

The above equation can be expressed in matrix form, as follows:

$$E(t)W(t) = 0$$

$$E(t) = [\varepsilon_1(t) \;\; \varepsilon_2(t) \;\; \varepsilon_3(t) \;\; \varepsilon_4(t)]$$

$$W(t) = [w_1(t) \;\; w_2(t) \;\; w_3(t) \;\; w_4(t)]^T \tag{31}$$

Based on Eq. (25) and Eq. (31), the weight of the last model in the convex can be calculated as $w_N = 1 - \sum_{i=1}^{N-1} w_i$. Thus, by subtracting the error $\varepsilon_N(\mathrm{t})$ of the *N*th model from both sides of Eq. (25), the following equations can be derived:

$$E_R(t)W_R(t) = -\varepsilon_4(t)$$

$$E_R(t) = [\varepsilon_1(t) - \varepsilon_4(t) \cdots \varepsilon_3(t) - \varepsilon_4(t)]$$

$$W_R(t) = [w_1(t) \;\; w_2(t) \;\; w_3(t)]^T \tag{32}$$

The above equations lay the foundation for the adaptive identification of w_i. By moving the term on the right side of the first equation in Eq. (32) to the left and multiplying with $E_R(t)^T$, the following equation can be derived:

$$E_R^T(t)E_R(t)W_R(t) + E_R^T(t)\varepsilon_4(t) = 0 \tag{33}$$

Now we are in the position to propose the adaptive identification law for the weights of the vertexes.

Theorem: Assume that the actual weights of the vertex models at time *t* are $W_R(t)$, the estimated weights are $\hat{W}_R(t)$, then the estimation error of weights can be expressed as $\tilde{W}_R = \hat{W}_R - W_R$. This value can converge to zero if the estimated weights has the following gradient descent based identification law:

$$\dot{\hat{W}}_R(t) = -\Gamma E_R^T(t)E_R(t)\hat{W}_R(t) - \Gamma E_R^T(t)\varepsilon_N(t)$$

$$\hat{w}_4(t) = 1 - \sum_{i=1}^{3} \hat{w}_i(t) \tag{34}$$

where Γ is a symmetric positive definite matrix to adjust the convergence speed.

Proof: Substitute the term $\tilde{W}_R = \hat{W}_R - W_R$into the first equation in Eq. (32), the following equation can be derived.

$$E_R\tilde{W}_R = E_R\hat{W}_R + \varepsilon_4 \tag{35}$$

To prove the convergence ability of the proposed adaptive law, define Lyapunov function as:

$$V\left(\tilde{W}_R(t)\right) = \frac{1}{2}\tilde{W}_R^T(t)\Gamma^{-1}\tilde{W}_R(t) \tag{36}$$

By combining Eq. (35)-Eq. (36), the following equation is derived:

$$\dot{\tilde{W}}_R(t) = \dot{\hat{W}}_R(t) = -\Gamma E_R^T(t)E_R(t)\tilde{W}_R(t) \tag{37}$$

Differentiate the Lyapunov function in Eq. (36), then integrate with Eq. (37), the following equation is derived:

$$\frac{dV\left(\tilde{W}_R(t)\right)}{dt} = -\left\|E_R(t)\tilde{W}_R(t)\right\|^2 \le 0 \tag{38}$$

In this way, the convergence of the estimation error under the proposed adaptive law has been proved.

However, although the proposed adaptive law have convergence ability and satisfy the first condition $\sum_{i=1}^{4} w_i(t) = 1$in Eq. (26), the second condition $w_i(t) \ge 0$, i = *1,2,…, N* is not guaranteed. Thus, a parameter projection method is introduced to the adaptive law. Firstly, the conditions in Eq. (26) are rewritten as follows:

$$S = \left\{\hat{W}_R \in R^3 | g\left(\hat{W}_R\right) \le 0\right\} \tag{39}$$

The function *g*() has the following definition to ensure the convergence ability:

$$g(\eta) = -\min\left\{\eta_1, \eta_2, \eta_3, 1 - \sum_{1}^{3}\eta_i\right\} \tag{40}$$

where η=[η_1,…η_{N-1}].

Define S^0 and ∂S as the interior and the boundary of S, respectively. Then the adaptive law can be revised as follows by applying the gradient projection method [53]:

$$\text{If } \left(\hat{W}_R \in S^0\right) \; or \; \left(\hat{W}_R \in \partial S \text{and} \hat{W}_R^T\nabla g \le 0\right):$$

$$\dot{\hat{W}}_R = -\Gamma\left(E_R^T\varepsilon_4 + E_R^T E_R\hat{W}_R\right)$$

Otherwise:

$$\dot{\hat{W}}_R = -\Gamma\left(E_R^T\varepsilon_4 + E_R^T E_R\hat{W}_R\right)$$

$$+ \Gamma\nabla g\left(\nabla g^T\Gamma\nabla g\right)^{-1}\nabla g^T\Gamma\left(E_R^T\varepsilon_N + E_R^T E_R\hat{W}_R\right) \tag{41}$$

where ∇g is the partial differential of g to the terms in η. For example, if η_1 is the minimum in η, then g(η) = $-\eta_1$, and ∇gshould be $[-1, 0 \ldots 0]_{N\text{-}1}$.

It is worth mentioning that compared with the robust methods, which are the classical way to deal with the uncertainties of tire cornering stiffness, the proposed multiple-model adaptive algorithm does not suffer from conservativeness.

IV. Simulation and Discussion

In order to evaluate the performance of the proposed method, simulations based on Carsim-Simulink co-simulation platform are conducted. The control algorithm is established in Matlab/Simulink and the vehicle is provided by Carsim. Here, the E-class hatchback in Carsim is utilized for simulation, and its parameters are listed in Table I. For a comprehensive evaluation, two cases are provided in the simulation. The first case is to show the improvement brought by the multiple model adaptive theory while the second case is to verify the effectiveness and superiority of the proposed controller.

Authorized licensed use limited to: University of Maryland College Park. Downloaded on October 10,2021 at 16:55:00 UTC from IEEE Xplore. Restrictions apply.

TABLE I
PARAMETER USED IN SIMULATION

Symbol	Definition	values
m	Vehicle mass	1650 kg
l_f	Distances of the front axle to the mass center	1.400 m
l_r	Distances of the rear axle to the mass center	1.650 m
I_z	Vehicle moment of inertial	3234 kgm^2
C_{f0}	Cornering stiffness of front tires (nominal value)	117000 N/rad
C_{r0}	Cornering stiffness of rear tires (nominal value)	108000 N/rad

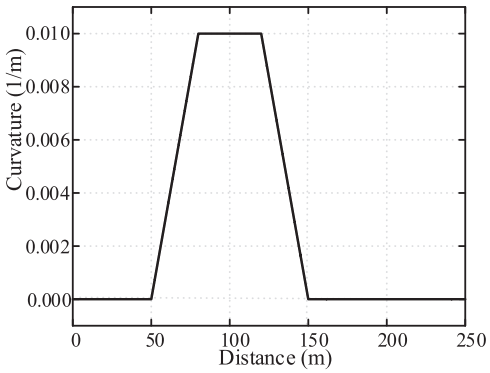

Fig. 9. Curvature of the J-turn maneuver.

A. Case One

In this scenario, the vehicle is made to conduct a J-turn maneuver at a speed of 90 km/h on road with relatively high adhesive condition (road coefficient: $\mu = 0.7$), the curvature of the reference path is shown in Fig. 9. And the holistic model predictive controller without the multiple-model adaptive law is introduced for comparison.

The path following performance is shown in Fig. 10, including the lateral error in Fig. 10(a), heading error in Fig. 10(b) and the global trajectory in Fig. 10(c). One can see that both the two controllers have satisfactory performance, the errors are constrained in a very small range and the differences between the reference path and the actual path are almost negligible. However, it can still observe from this figure that the controller with multiple model adaptive law has better performance than the nominal controller. This improvement can be attributed to the fact that the multiple model adaptive law enhances the internal model accuracy of the controller.

To better illustrate the results, the quantitative analysis is introduced which utilizes the root mean square (RMS) value as the tool. Here, the RMS values of lateral errors and head errors are compared, as shown in Table II. The "relative ratio" is the percentage of MMAPC in MPC. Although the RMS values reflect the whole case including the straight line, one can still see that the improvement brought by multiple model adaptive method is evident.

The dynamics parameters including the yaw rate and side slip angle are shown in Fig. 11. It is shown that the values are all in the reasonable ranges. Although the performance of the two

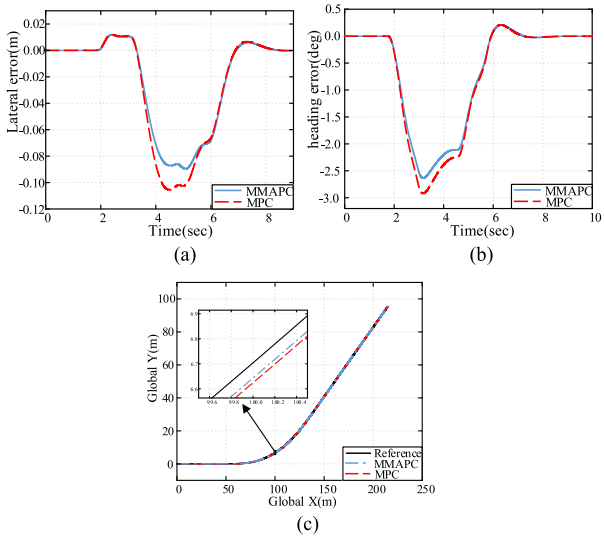

Fig. 10. Path following performance: (a) Lateral error, (b) Heading error, (c) Global trajectory.

TABLE II
ROOT MEAN SQUARE VALUE COMPARISON

Controller	Lateral error	Heading error
MMAPC	0.03941	1.1542
MPC	0.04545	1.2162
Relative ratio	86.7%	94.9%

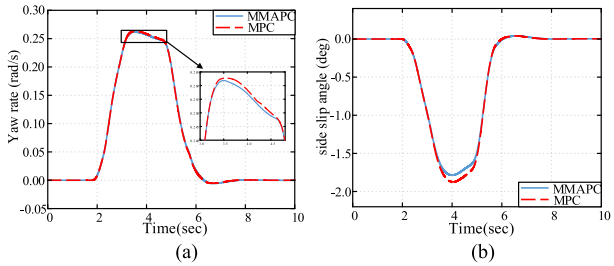

Fig. 11. Dynamics responses: (a) Yaw rate, (b) Side slip angle.

controllers are quite similar, it can be seen from Fig. 11(b) that the side slip angle of the adaptive predictive controller is a little bit smaller than the nominal controller, which also reflects the effect of the adaptive algorithm. These results have shown that the controllers can easily complete the path following objective with excellent performance, while the control inputs and the slip ratio of wheels are all in normal range, so their values are omitted here. Since the maneuver conducted in this scenario is already quite aggressive compared to most driving conditions of the on-road vehicles [54], it is persuasive to conclude that the performance of the proposed method on normal conditions has been verified.

B. Case Two

To further evaluate the effectiveness and features of the proposed method, an extreme driving condition is provided in this case, as shown in Fig. 12(a). The scenario is designed as follows: The vehicle is driving at a very high speed of 120 km/h under

Authorized licensed use limited to: University of Maryland College Park. Downloaded on October 10,2021 at 16:55:00 UTC from IEEE Xplore. Restrictions apply.

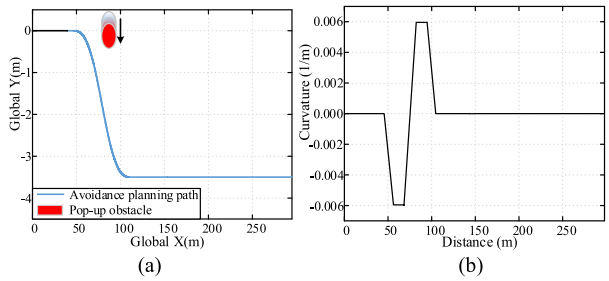

Fig. 12. The reference path and its curvature: (a) Reference path, (b) Curvature.

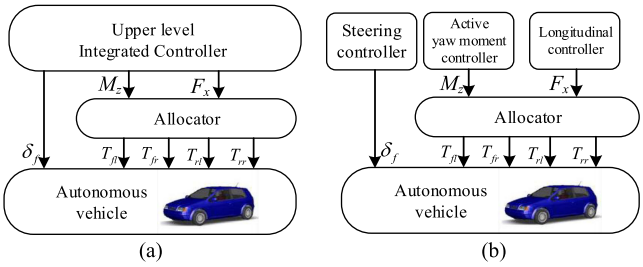

Fig. 13. Rough follow charts: (a) Controller with hierarchical structure, (b) Controller with separate structure.

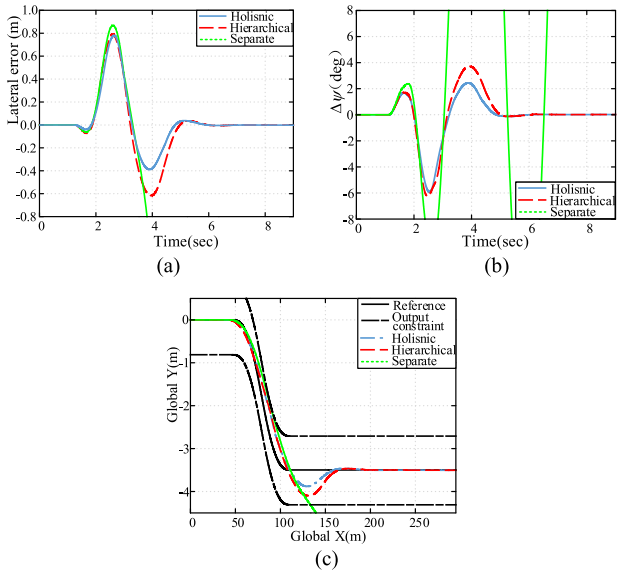

Fig. 14. Path following performance: (a) lateral error, (b) heading error, (c) global trajectory.

TABLE III
ROOT MEAN SQUARE VALUE COMPARISON

Controller	Lateral error	Heading error
Holistic	0.281	1.765
Hierarchical	0.328	1.963
Relative ratio	85.6%	89.7%

slipper road (road coefficient: $\mu = 0.3$), suddenly an obstacle appears from the left side (the red/gray ellipse in Fig. 12(b)), so an avoidance lane-change path (blue line in Fig. 12(a)) is planned for collision avoidance. Since this study focuses on the path following problem, the path planning process is not discussed here. The curvature of the reference planning path is shown in Fig. 12(b).

Two other controllers are introduced for comparison. The first one is an integrated controller with a classical hierarchical structure, the upper-level controller calculates the steering angle and the two generalized forces (F_{xt} and M_z) while a lower-level tire force allocator allocate the generalized forces to each tire. The second one is a controller with separate structure, the steering angle and the generalized forces are calculated separately, and there is also a lower-level allocator for force distribution. The rough flow charts of the two controllers are demonstrated in Fig. 13, the hierarchical structure is shown in Fig. 13(a) and Fig. 13(b) shows the separate structure.

Fig. 14 shows the path following performance. One can see from this figure that the condition is very extreme and it is impossible to track the reference path with high accuracy. The controller with separate structure fails to track the avoidance path and has lost its controllability during the maneuver. While the controllers with holistic structure and hierarchical structure are still able to complete the path following objective, and it can be observed from the trajectory in Fig. 14 that the errors of the two controllers are within the output constraints defined in MPC, which can help ensure the road safety. However, it is obvious that the controller with holistic structure can achieve better performance than the controller with hierarchical structure, both the lateral error and heading error are smaller. This is because in extreme conditions, owing to the longitudinal slip characteristic of tires, the actuators may have difficulties to fulfill the generalized forces calculated by upper-level controller. But for the controller with holistic structure, the control output on each corner is calculated directly without the generalized forces as the intermediate variables. So the problem in the hierarchical structure can be well solved, which shows the superiority of the holistic structure in the path following control of autonomous vehicle.

The RMS value comparison of this case is shown in Table III. Since the controller with separate structure fails to complete the maneuver, the quantitative comparison is only conducted between holistic structure and hierarchical structure. It can be seen from the results that the proposed controller with holistic structure can evidently improve the control performance compared with classical algorithm based on hierarchical structure.

The dynamics responses of vehicle including the yaw rate, side slip angle and longitudinal velocity are shown in Fig. 15. One can observe from this figure that the controller with separate structure has lost its dynamics stability, this can also illustrate why it cannot correct the position of vehicle in Fig. 14. For the controllers with the hierarchical structure and the holistic structure, although the side slip angles are relatively large compared with case one, the values are still reasonable and the dynamics stability of vehicle can be guaranteed. Moreover, it can be seen from Fig. 15(c) that owing to the weight adaptive mechanism for system outputs, the longitudinal velocity deviates from its reference value when the lateral controller encounters difficulties to fulfill its tasks, and after the extreme maneuver has been finished for a time lag, the velocity can quickly track

Authorized licensed use limited to: University of Maryland College Park. Downloaded on October 10,2021 at 16:55:00 UTC from IEEE Xplore. Restrictions apply.

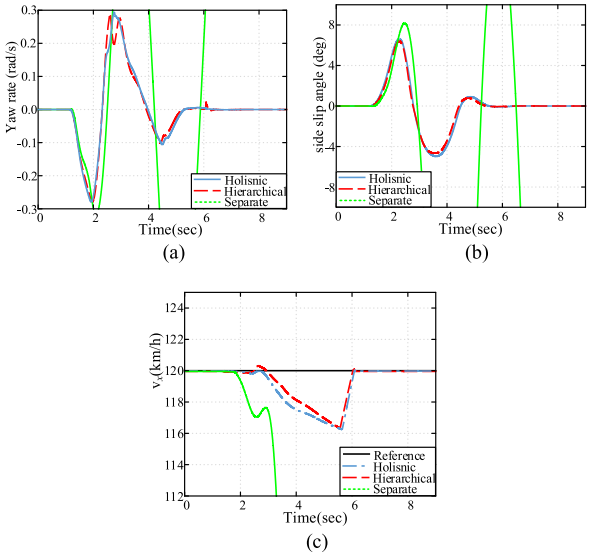

Fig. 15. Dynamics responses: (a) yaw rate, (b) lateral velocity, (c) longitudinal velocity.

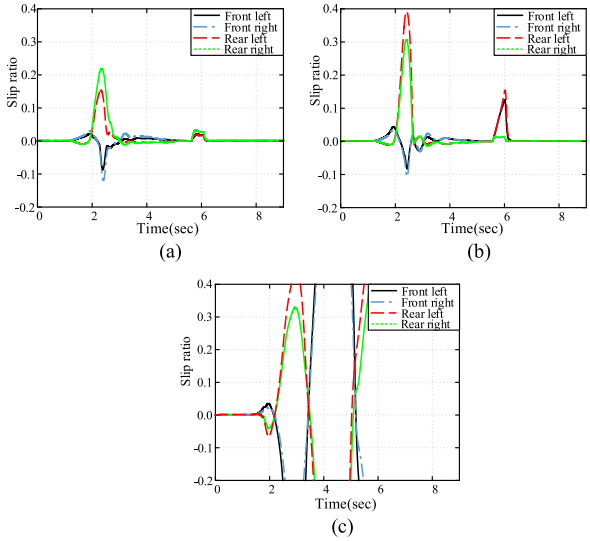

Fig. 17. Slip ratio: (a) holistic controller, (b) hierarchical controller, (c) separate controller,

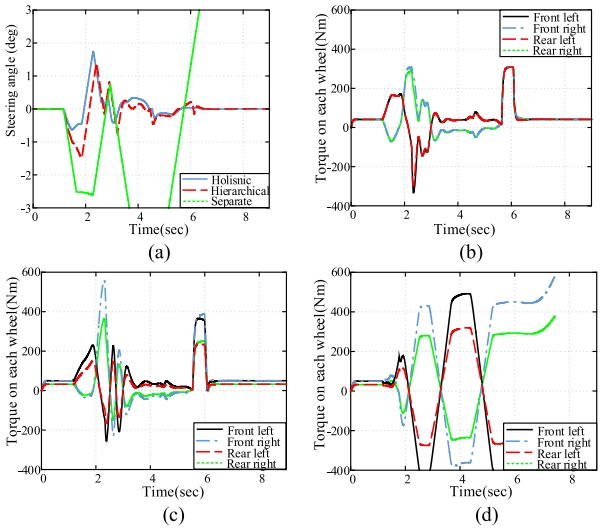

Fig. 16. Control output: (a) steering angle, (b) torques of the holistic controller, (c) torques of the hierarchical controller, (d) torques of the separate controller.

its reference value again. In this way, a lateral-longitudinal cooperating mechanism for extreme conditions is realized.

The control outputs are shown in Fig. 16. It is shown that the control outputs of the separate structure based controller are seriously oversized and the vehicle is out of control when no cooperation exists between the sub-systems in this extreme condition. The control outputs of the controllers based on the holistic structure and the hierarchical structure are still in reasonable range. But one can observe that the torque outputs of the controller based on the holistic structure are generally smaller and smoother than the controller based on the hierarchical structure.

The results of slip ratio at each corner are shown in Fig. 17. One can see that the slip ratios of the controller with separate structure are totally out of control. And it is shown that the slip ratios of the controller based on hierarchical structure are seriously oversized beyond the normal ranges, while the controller based on holistic structure can maintain its slip ratios within the normal ranges during the whole maneuver, which also shows the superiority of the proposed holistic structure. Although some researches about hierarchical controller on vehicle dynamics control introduced a servo controller to constraint the slip ratio of vehicle [55]–[56], the conflicts between upper-level controller and the actuators still cannot be solved [57]. In this regard, the proposed holistic path following controller has irreplaceable advantages over previous researches.

V. Conclusion

A novel holistic adaptive multi-model predictive path following controller for 4WID autonomous vehicle was proposed in this paper. The controller has a linear structure since the complex relationships in the model are well decoupled, which is very beneficial for the real time performance of MPC. A weight adaptive mechanism was designed to ensure that the proposed controller can handle extreme conditions. In addition, a multi-model adaptive law was introduced for the tire cornering stiffness uncertainties. Comprehensive case-studies were conducted to verify the effectiveness of the proposed method. The results show that the proposed controller can achieve excellent performance in both normal and extreme driving conditions. In normal conditions, the path following error is negligible and the multiple-model adaptive law can effectively improve the performance. While in extreme driving conditions, the weighting adaptive mechanism can help maintain the road safety and the dynamics stability. The superiority of the proposed holistic structure over other control structures of 4WID autonomous vehicle was also demonstrated.

Future focus will be put on the fault-tolerant mechanism design for the proposed method, the integration of planning and tracking, and finally evaluating in a real vehicle to investigate its real-world performance.

Authorized licensed use limited to: University of Maryland College Park. Downloaded on October 10,2021 at 16:55:00 UTC from IEEE Xplore. Restrictions apply.

REFERENCES

[1] K. Talvala, K. Kritayakirana, and J. Gerdes, "Pushing the limits: From lanekeeping to autonomous racing," *Annu. Rev. Control.*, vol. 35, no. 1, pp. 137–148, Apr. 2011.

[2] M. Anderson *et al.*, *Autonomous Vehicle Technology: A Guide for Policymakers*, Santa Monica, CA, USA: Rand Corp., 2014.

[3] Y. Chen, C. Hu, and J. Wang, "Human-centered trajectory tracking control for autonomous vehicles with driver cut-in behavior prediction," *IEEE Trans. Veh. Technol*, vol. 68, no. 9, pp. 8461–8471, Sep. 2019.

[4] Y. Huang *et al.*, "A motion planning and tracking framework for autonomous vehicles based on artificial potential field elaborated resistance network approach," *IEEE Trans. Ind. Electron.*, vol. 67, no. 2, pp. 1376–1386, Feb. 2020.

[5] R. Marino, S. Scalzi, and M. Netto, "Nested PID steering control for lane keeping in autonomous vehicles," *Control. Eng. Pract.*, vol. 19, no. 12, pp. 1459–1467, Dec. 2011.

[6] W. Wang, T. Hsu, and T. Wu, "The improved pure pursuit algorithm for autonomous driving advanced system," in *Proc. IEEE 10th Int. Workshop Comput. Intell. Appl.*, Hiroshima, 2017, pp. 33–38.

[7] A. Nguyen, C. Sentouh, H. Zhang, and J. Popieul, "Fuzzy static output feedback control for path following of autonomous vehicles with transient performance improvements," *IEEE Trans. Intell. Transp. Syst.*, vol. 21, no. 7, pp. 3069–3079, Jul. 2020.

[8] C. Hu, R. Wang, and F. Yan, "Integral sliding mode-based composite nonlinear feedback control for path following of four-wheel independently actuated autonomous vehicles," *IEEE Trans. Transp. Electron.*, vol. 2, no. 2, pp. 221–230, Jun. 2016.

[9] S. Xu and H. Peng, "Design, analysis, and experiments of preview path tracking control for autonomous vehicles," *IEEE Trans. Intell. Transp. Syst.*, vol. 21, no. 1, pp. 48–58, Jan. 2020.

[10] S. Xu, H. Peng, and Y. Tang, "Preview path tracking control with delay compensation for autonomous vehicles," *IEEE Trans. Intell. Transp. Syst.*, early access, 2020, doi: 10.1109/TITS.2020.2978417.

[11] K. Berntorp *et al.*, "Trajectory tracking for autonomous vehicles on varying road surfaces by friction-adaptive nonlinear model predictive control," *Veh. Syst. Dyn.*, vol. 58, no. 5, pp. 705–725, Nov. 2019.

[12] G. V. Raffo, G. K. Gomes, J. E. Normey-Rico, C. R. Kelber, and L. B. Becker, "A predictive controller for autonomous vehicle path tracking," *IEEE Trans. Intell. Transp. Syst.*, vol. 10, no. 1, pp. 92–102, Mar. 2009.

[13] H. Guo *et al.*, "Model predictive path following control for autonomous cars considering a measurable disturbance: Implementation, testing, and verification," *Mech. Syst. Signal Process.*, vol. 118, pp. 41–60, Mar. 2019.

[14] J. Theunissen *et al.*, "Regionless explicit model predictive control of active suspension systems with preview," *IEEE Trans. Ind. Electron.*, vol. 67, no. 6, pp. 4877–4888, Jun. 2020.

[15] L. H. Csekő, M. Kvasnica, and B. Lantos, "Explicit MPC-based RBF neural network controller design with discrete-time actual kalman filter for semiactive suspension," *IEEE Trans. Control. Syst. Technol.*, vol. 23, no. 5, pp. 1736–1753, Sep. 2015.

[16] C. E. Beal and J. C. Gerdes, "Model predictive control for vehicle stabilization at the limits of handling," *IEEE Trans. Control. Syst. Technol.*, vol. 21, no. 4, pp. 1258–1269, Jul. 2013.

[17] L. Zhai *et al.*, "Electronic stability control based on motor driving and braking torque distribution for a four in-wheel motor drive electric vehicle," *IEEE Trans. Veh. Technol.*, vol. 65, no. 6, pp. 4726–4739, Jun. 2016.

[18] B. Zhao *et al.*, "Stability control of electric vehicles with in-wheel motors by considering tire slip energy," *Mech. Syst. Signal Process.*, vol. 118, pp. 340–359, Mar. 2019.

[19] Y. Liang *et al.*, "Integrated lateral control for 4WID/4WIS vehicle in high-speed condition considering the magnitude of steering," *Veh. Syst. Dyn.*, 2019, doi: 10.1080/00423114.2019.1645343.

[20] Q. Lu *et al.*, "Enhancing vehicle cornering limit through sideslip and yaw rate control," *Mech. Syst. Signal Process.*, vol. 75, pp. 455–472, Jun. 2016.

[21] H. Jing *et al.*, "Robust H∞ dynamic output-feedback control for four-wheel independently actuated electric ground vehicles through integrated AFS/DYC," *J. Franklin Inst.*, vol. 355, no. 18, pp. 9321–9350, Dec. 2018.

[22] S. Çağlar Baslamisli, İ. E. Köse, and G. Anlaş, "Gain-scheduled integrated active steering and differential control for vehicle handling improvement," *Veh. Syst. Dyn.*, vol. 14, no. 1, pp. 99–119, Dec. 2018.

[23] R. Wang, H. Zhang, and J. Wang, "Linear parameter-varying controller design for four-wheel independently actuated electric ground vehicles with active steering systems," *IEEE Trans. Control. Syst. Technol.*, vol. 22, no. 4, pp. 1281–1296, Jul. 2014.

[24] R. Wang *et al.*, "Robust lateral motion control of four-wheel independently actuated electric vehicles with tire force saturation consideration," *J. Franklin Inst.*, vol. 352, no. 2, pp. 645–668, Dec. 2015.

[25] H. Zhang and W. Zhao, "Decoupling control of steering and driving system for in-wheel-motor-drive electric vehicle," *Mech. Syst. Signal Process.*, vol. 101, pp. 389–404, Feb. 2018.

[26] H. Zhao *et al.*, "Modular integrated longitudinal, lateral, and vertical vehicle stability control for distributed electric vehicles," *IEEE Trans. Veh. Technol.*, vol. 68, no. 2, pp. 1327–1338, Feb. 2019.

[27] J. Zhu *et al.*, "Braking/steering coordination control for in-wheel motor drive electric vehicles based on nonlinear model predictive control," *Mechanism Mach. Theory*, vol. 142, Dec. 2019, Art. no. 103586.

[28] H. Zhao *et al.*, "Modular integrated longitudinal, lateral, and vertical vehicle stability control for distributed electric vehicles," *IEEE Trans. Veh. Technol.*, vol. 68, no. 2, pp. 1327–1338, Feb. 2019.

[29] C. Chatzikomis *et al.*, "Comparison of path tracking and torque-vectoring controllers for autonomous electric vehicles," *IEEE Trans. Intell. Veh.*, vol. 3, no. 4, pp. 559–570, Dec. 2018.

[30] Y. Ren, L. Zheng, and A. Khajepour, "Integrated model predictive and torque vectoring control for path tracking of 4-wheel-driven autonomous vehicles," *IET Intell. Transport Syst.*, vol. 13, no. 1, pp. 98–107, Jan. 2019.

[31] A. Goodarzi, A. Sabooteh, and F. Esmailzadeh, "Automatic path control based on integrated steering and external yaw-moment control," *Proc. Inst. Mech Eng Pt K-J Multi-Body Dyn.*, vol. 222, no. 2, pp. 189–200, Dec. 2018.

[32] C. Hu, R. Wang, F. Yan, and N. Chen, "Output constraint control on path following of four-wheel independently actuated autonomous ground vehicles," *IEEE Trans. Veh. Technol.*, vol. 65, no. 6, pp. 4033–4043, Jun. 2016.

[33] R. Wang *et al.*, "Composite nonlinear feedback control for path following of four-wheel independently actuated autonomous ground vehicles," *IEEE Trans. Intell. Transp. Syst.*, vol. 17, no. 7, pp. 2063–2074, Jul. 2016.

[34] J. Guo, Y. Luo, K. Li, and Y. Dai, "Coordinated path-following and direct yaw-moment control of autonomous electric vehicles with sideslip angle estimation," *Mech. Syst. Signal Pr.*, vol. 105, pp. 183–199, May. 2018.

[35] T. Kobayashi *et al.*, "Efficient direct yaw moment control: Tyre slip power loss minimisation for four-independent wheel drive vehicle," *Veh. Syst. Dyn.*, vol. 56, no. 5, pp. 719–733, May 2017.

[36] M. Ataei, A. Khajepour, and S. Jeon, "Model predictive control for integrated lateral stability, traction/braking control, and rollover prevention of electric vehicles," *Veh. Syst. Dyn.*, vol. 58, no. 1, pp. 49–73, Mar. 2019.

[37] H. Zhou, F. Jia, H. Jing, Z. Liu, and L. Güvenç, "Coordinated longitudinal and lateral motion control for four wheel independent motor-drive electric vehicle," *IEEE Trans. Veh. Technol.*, vol. 67, no. 5, pp. 3782–3790, May 2018,.

[38] B. Ren *et al.*, "MPC-based yaw stability control in in-wheel-motored EV via active front steering and motor torque distribution," *Mechatronics*, vol. 38, pp. 103–144, Sep. 2016.

[39] L. Yuan *et al.*, "Nonlinear MPC-based slip control for electric vehicles with vehicle safety constraints," *Mechatronics*, vol. 38, pp. 1–15, Sep. 2016.

[40] M. Jalali *et al.*, "Integrated model predictive control and velocity estimation of electric vehicles," *Mechatronics*, vol. 46, pp. 84–100, Oct. 2017.

[41] J. Funke, M. Brown, S. M. Erlien, and J. C. Gerdes, "Collision avoidance and stabilization for autonomous vehicles in emergency scenarios," *IEEE Trans. Control. Syst. Technol.*, vol. 25, no. 4, pp. 1204–1216, Jul. 2017.

[42] H. Guo *et al.*, "Dual-envelop-oriented moving horizon path tracking control for fully automated vehicles," *Mechatronics*, vol. 50, pp. 422–433, Jan. 2018.

[43] M. Brown *et al.*, "Safe driving envelopes for path tracking in autonomous vehicles," *Control Eng. Pract.*, vol. 61, pp. 307–316, Apr. 2017.

[44] X. He *et al.*, "Emergency steering control of autonomous vehicle for collision avoidance and stabilization," *Veh. Syst. Dyn.*, vol. 57, no. 8, pp. 1163–1187, Nov, 2018.

[45] K. Guo and D. Lu, "UniTire: Unified tire model for vehicle dynamic simulation," *Veh. Syst. Dyn.*, vol. 45, no. S1, pp. 79–99, Mar. 2018.

[46] J. Guo *et al.*, "Robust lateral control of autonomous four-wheel independent drive electric vehicles considering the roll effects and actuator faults," *Mech. Syst. Signal Process.*, vol. 143, Sep. 2020, Art. no. 106773.

[47] C. Hu, H. Jing, R. Wang, F. Yan, and M. Chadli, "Robust H∞ output-feedback control for path following of autonomous ground vehicles," *Mech. Syst. Signal Process.*, vol. 70/71, pp. 414–427, Sep. 2015.

[48] R. Wang, H. Jing, C. Hu, F. Yan, and N. Chen, "Robust H∞ path following control for autonomous ground vehicles with delay and data dropout," *IEEE Trans. Intell. Transp. Syst.*, vol. 17, no. 7, pp. 2042–2050, Jul. 2016.

Authorized licensed use limited to: University of Maryland College Park. Downloaded on October 10,2021 at 16:55:00 UTC from IEEE Xplore. Restrictions apply.

[49] J. Suh, H. Chae, and K. Yi, "Stochastic model-predictive control for lane change decision of automated driving vehicles," *IEEE Trans. Veh. Technol.*, vol. 67, no. 6, pp. 4771–4782, Jun. 2018.
[50] R. Rajamani, *Vehicle Dynamics and Control*, Berlin, Germany: Springer Science, 2006.
[51] H. Zengin, N. Zengin, B. Fidan, and A. Khajepour, "Blending based multiple-model adaptive control for multivariable systems and application to lateral vehicle dynamics," in *Proc. 18th Eur. Control Conf.*, Naples, Italy, 2019, pp. 2957–2962.
[52] P. Ioannou and B. Fidan, "Adaptive control tutorial," *Soc. for Ind. Appl. Math.*, Philadelphia, United States, vol. 11, 2006.
[53] Zengin H., "Multiple-model robust adaptive vehicle motion control," Ph.D. dissertation, Univ. Waterloo, Waterloo, Canada, 2019.
[54] C. Hu *et al.*, "MME-EKF-based path-tracking control of autonomous vehicles considering input saturation," *IEEE Trans. Veh. Technol.*, vol. 68, no. 6, pp. 5246–5259, Jun. 2019.
[55] E. Joa *et al.*, "A tyre slip-based integrated chassis control of front/rear traction distribution and four-wheel independent brake from moderate driving to limit handling," *Veh. Syst. Dyn.*, vol. 56, no. 4, pp. 579–603, Nov. 2017.
[56] Y. Wang, H. Fujimoto, and S. Hara, "Driving force distribution and control for EV with four In-wheel motors: A case study of acceleration on split-friction surfaces," *IEEE Trans. Ind. Electron.*, vol. 64, no. 4, pp. 3380–3388, Apr. 2017.
[57] M. Jaladi *et al.*, "Integrated stability and traction control for electric vehicles using model predictive control," *Control Eng. Pract.*, vol. 54, pp. 256–266, Sep. 2016.

Yixiao Liang received the B.S. degree in 2016 from Chongqing University, Chongqing, China, where he is currently working toward the Ph.D. degree with the School of Automotive Engineering. He is currently a Visiting Ph.D. Student with the Department of Mechanical and Mechatronics Engineering, University of Waterloo, Waterloo, ON, Canada. His research interests include vehicle dynamics and control, and autonomous vehicle.

Yinong Li received the B.Tech. degree from Changan University, Xian, China, in 1983, the M.S. degree from Chongqing University, Chongqing, China, in 1993, and the Ph.D. degree from Northeastern University, Shenyang, China, in 1999. He is currently a Professor with the School of Automotive Engineering, Chongqing University. He has authored more than 200 papers. His research interests include vehicle dynamics and control for intelligent electric vehicles, and vibration active control. He was the Director of the Society of Vibration Engineering of China. He was on the Editorial Boards of the Journal of Automotive Engineering and the Journal of Vibration Engineering.

Amir Khajepour is a Professor with the Department of Mechanical and Mechatronics Engineering, University of Waterloo, Waterloo, ON, Canada. He has applied his expertise in several key multidisciplinary areas including system modeling and the control of dynamic systems. His research has resulted in many patents and technology transfers. He is the author of more than 400 journal and conference publications, as well as several books. He holds the Canada Research Chair in Mechatronic Vehicle Systems and Senior NSERC/General Motors Industrial Research program in Holistic Vehicle Control. He is a Fellow of the Engineering Institute of Canada, the American Society of Mechanical Engineers, and the Canadian Society for Mechanical Engineering and technology transfers.

Ling Zheng received the B.S., M.S., and Ph.D. degrees from Chongqing University, Chongqing, China, in 1984, 1989, and 2005, respectively. She is currently a Professor with the School of Automotive Engineering, Chongqing University. She has authored more than 100 papers. Her research interests include advanced driving-assistant system design and control in vehicle, semiactive and active vibration and noise control, dynamic behavior mechanism, and optimal control in automated vehicle. She was an Associate Editor for the *Journal of Advances in Mechanical Engineering*.

Authorized licensed use limited to: University of Maryland College Park. Downloaded on October 10,2021 at 16:55:00 UTC from IEEE Xplore. Restrictions apply.